ACS OMEGA

http://pubs.acs.org/journal/acsodf

Article

Insights into the Factors Controlling the Origin of Activation Barriers in Group 13 Analogues of the Four-Membered N-Heterocyclic Carbenes

Zheng-Feng Zhang and Ming-Der Su*

Cite This: *ACS Omega* 2021, 6, 22272−22283

Read Online

ACCESS | Metrics & More | Article Recommendations | Supporting Information

ABSTRACT: The mechanisms of C−H bond insertion and alkene cycloaddition were investigated theoretically using five model systems: group 13 analogues of the four-membered nucleophilic *N*-heterocyclic carbenes (NHCs) (**1E**; E = group 13 element). The theoretical findings indicate that, except for **1B** with $H_2C{=}CH_2$, these four-membered NHCs undergo insertion and [1 + 2] cycloaddition reactions with difficulty because their activation barriers are quite high (31 kcal/mol). The theoretically confirmed chemical inertness of the four-membered NHCs **1Ga** and **1In** might explain why they have been experimentally detected at room temperature. Additionally, our theoretical observations indicate that the reactivity of these four-membered NHCs featuring a central group 13 element follows the order **1B** ≫ **1Al** > **1Ga** > **1In** > **1Tl**. The theoretical examination suggests that the smaller the atomic radius of the central group 13 element in the four-membered NHC analogue is, the larger the aromaticity of this carbenic molecule is, the higher the basicity of this carbenic molecule in nature is, the larger its nucleophilic attack on other oncoming molecules is, the smaller the barrier heights of its C−H bond insertion and [1 + 2] cycloaddition reactions will be, the higher its exothermicities for these products will be, and thus, the greater its reactivity will be. Moreover, the present theoretical findings reveal that the reactivity of **1B** is governed by its highest occupied molecular orbital, a nonbonding sp^2 lone pair orbital. In contrast, the reactivity of the four heavier **1E′** (E′ = Al, Ga, In, and Tl) molecules is mainly determined by their lowest unoccupied molecular orbital, a vacant p−π orbital. The conclusions gained from this study allow many predictions to be made.

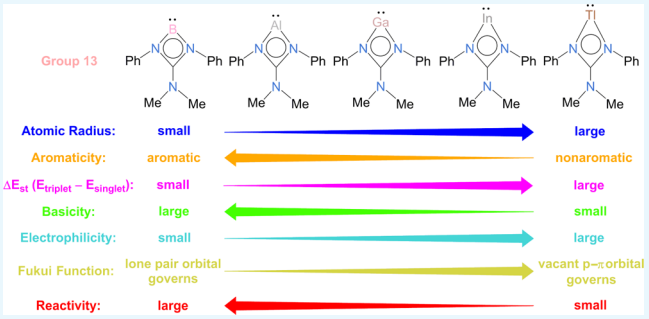

1. INTRODUCTION

Carbene is a molecule that features a neutral dicoordinate carbon atom with only six electrons in its valence shell.[1] Carbenes were conventionally known to be short-lived, very reactive, and thus extremely difficult to stabilize in the laboratory.[1] Thanks to Arduengo, Harlow, and Kline,[2] the above traditional view has been dramatically altered with the availability of heteroatom-stabilized singlet nucleophilic *N*-heterocyclic carbenes (NHCs), which can be isolated at an ambient air temperature and used as general reagents. Thus, not surprisingly, carbene chemistry has undergone a renaissance during the last 3 decades.[3−7] To date, many room-temperature-stable NHCs have been experimentally synthesized and structurally characterized to allow their properties to be scrutinized in all respects.[8−19]

Through the distinguished efforts of Jones and co-workers,[20] the first four-membered-ring NHC analogues containing a group 13 element E (E = B, Al, Ga, In, and Tl) have been stabilized and isolated. These neutral NHCs have been verified for Ga and In, as shown in Scheme 1.[20] These two compounds are kinetically stabilized by the incorporation of a very bulky and electron-rich guanidinate ligand, that is, {[N-(Ar)]$_2$CNCy$_2$} (Cy = cyclohexyl).[20] As a result, in the solid state, each compound has been demonstrated via X-ray crystallography to have a two-coordinate center (Ga or In),

Scheme 1. Experimentally Reported Molecular Structure[a]

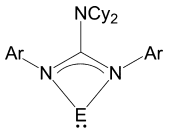

E = Ga, In
Ar = $C_6H_3Pr^i_2$-2,6
Cy = cyclohexyl

[a]See ref 20.

Received: June 6, 2021
Accepted: August 13, 2021
Published: August 20, 2021

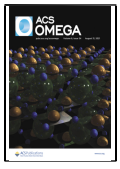

ACS Publications

© 2021 The Authors. Published by American Chemical Society

Table 1. Geometrical Parameters (in Å and Degrees) and Some Physical Properties for 1E (E = Group 13 Elements) Optimized at the BP86[a]/def2-SVP[b] Level of Theory

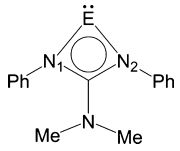

	1B	1Al	1Ga	1In	1Tl
E−N_1 (Å)[c]	1.502	2.061	2.163 [2.087]	2.378 [2.298]	2.488
E−N_2 (Å)[c]	1.502	2.061	2.163 [2.095]	2.378 [2.298]	2.488
∠N_1−E−N2 (°)[c]	87.88	65.62	63.81 [63.77]	57.78 [58.06]	54.63
ΔE_{st} (kcal mol^{-1})[d]	10.9	43.9	50.6	53.1	54.5
NICS(0) (ppm)[e]	−16.44	−2.511	−2.132	−1.935	−1.688
NICS(1) (ppm)[f]	−6.469	−1.515	−0.688	−0.597	−0.227
NICS(1)zz(ppm)[g]	−7.592	−4.155	−1.842	0.629	1.097
PA (kcal mol^{-1})[h]	302.2	249.0	229.4	217.6	200.6
GB (kcal mol^{-1})[i]	288.7	237.2	217.5	204.3	188.4
μ (eV)[j]	2.945	3.108	3.333	3.262	3.171
η (eV)[k]	5.890	6.216	6.665	6.524	6.342
ω (eV)[l]	0.736	0.777	0.833	0.816	0.793
f_k^{+}[m]	−0.187	−0.387	−0.480	−0.704	−0.813
f_k^{-}[n]	−0.479	−0.406	−0.193	−0.080	−0.085
f_k^{0}[o]	−0.333	−0.397	−0.337	−0.392	−0.449

[a]See refs 29 and 30. [b]See refs 31−33. [c]Experimental values in the square bracket are from ref 20. [d]Energy relative to the corresponding singlet state. A positive value means that the singlet is in the ground state. The Cartesian coordinates for **1E** at the lowest singlet and triplet states are given in the Supporting Information. [e]NICS(0) was computed at the center of the molecular plane. [f]NICS(1) was computed at 1.0 Å above the center of the molecular plane. [g]NICS(1)zz was computed at the zz component of the magnetic tensor NICS(1). [h]The proton affinity (PA) of **1E** is based on eq 3. [i]The gas-phase basicity (GB) of **1E** is based on eq 3. [j]μ represents the electronic chemical potential; see eq 4 and Table S3. [k]η represents the chemical hardness; see eq 5 and Table S3. [l]ω represents the electrophilicity index; see eq 6 and Table S3. [m]f_k^{+} represents the nucleophilic attack; see eq 7 and Table S4. [n]f_k^{-} represents the electrophilic attack; see eq 8 and Table S4. [o]f_k^{0} represents the radical attack; see eq 9 and Table S4.

which has no close inter- or intramolecular interactions.[20] To date, attempts to prepare the four-membered NHC analogues bearing either boron or aluminum central elements have been unsuccessful.[21] On the other hand, arranging the thallium analogue led to the isomeric N, Ar-chelated complex, [:Tl{h^1-N, h^3-Ar-[N(Ar)]$_2$CN(C_6H_{11})$_2$}],[20,22,23] presumably because of the larger atomic radius of Tl in this species. Theoretical studies[20−23] reported that each four-membered heterocycle possesses a lone pair of electrons at the group 13 E center (highest occupied molecular orbital, HOMO, with sp^2 character), which acts as a σ-donor. Additionally, the group 13 center of the four-membered NHCs has an empty π−π orbital [lowest unoccupied molecular orbital (LUMO)], which can be considered a π-acceptor. Therefore, these theoretical works strongly suggest that such four-membered heterocyclic NHCs with a central E element can be considered good σ-donor and weak π-acceptor ligands.[20−23] Based on these works, much experimental effort has been devoted to studying the structural and spectroscopic properties of the coordinated complexes arising from these four-membered group 13 NHC species with transition-metal fragments.[24−27] Nevertheless, so far neither experimental nor theoretical studies have been performed on the reactivity of these four-membered group 13 NHC analogues toward small organic molecules, let alone on comprehending the root of their reactivity. To gain a better understanding of the origin of the activation barriers of these four-membered group 13 NHC counterparts, we investigated computationally the C−H bond insertion (eq 1) and [1 + 2] cycloaddition (eq 2) reactions of **1E** with methane and ethene, respectively, using the density functional theory (DFT). For simplicity, however, we applied the phenyl and methyl substituents (Table 1) in **1E** rather than the original bulky substituents shown in Scheme 1.

$$\mathbf{1E} + CH_4 \rightarrow \mathbf{TS}\text{-}1\vec{\mathrm{E}}\mathbf{Prod}\text{-}1\mathrm{E} \quad (1)$$

$$\mathbf{1E} + C_2H_4 \rightarrow \mathbf{TS}\text{-}2\vec{\mathrm{E}}\mathbf{Prod}\text{-}2\mathrm{E} \quad (2)$$

E = B, Al, Ga, In, and Tl.

An intriguing question to be solved in this study is whether the aromatic (or antiaromatic) character of its four-membered ring affects the chemical reactivity of **1E**. Basically, but not in general, an aromatic ring in the geometrical structure of the NHC species plays a role[28] in stabilizing the entire carbenic system because traditional carbenes are notorious for being very reactive. This theoretical investigation demonstrates that the interplay of the central E and the electronic factors (including the aromaticity, basicity, and electrophilicity) of the four-membered carbenic ring can effectively establish the relative reactivity of these cyclic carbene systems, **1E**.

2. METHODOLOGY

All structures were fully optimized in the gas phase using DFT[29,30] with the BP86 functional and the standard def2-SVP basis set[31−33] for all atoms. Frequency calculations were performed at the same level of theory to confirm that all stationary points were minima (no imaginary frequency) or transition states (one imaginary frequency). Calculations of intrinsic reaction coordinates[34−36] were also performed on the transition states to confirm that these geometries indeed connected two relevant minima. For better energetics, we used the BP86-D3(BJ)[37,38]/def2-TZVPP[39] and M06-2X[40]-D3(BJ)/def2-TZVP[41] levels of theory based on the BP86/def2-SVP

https://doi.org/10.1021/acsomega.1c02958
ACS Omega 2021, 6, 22272−22283

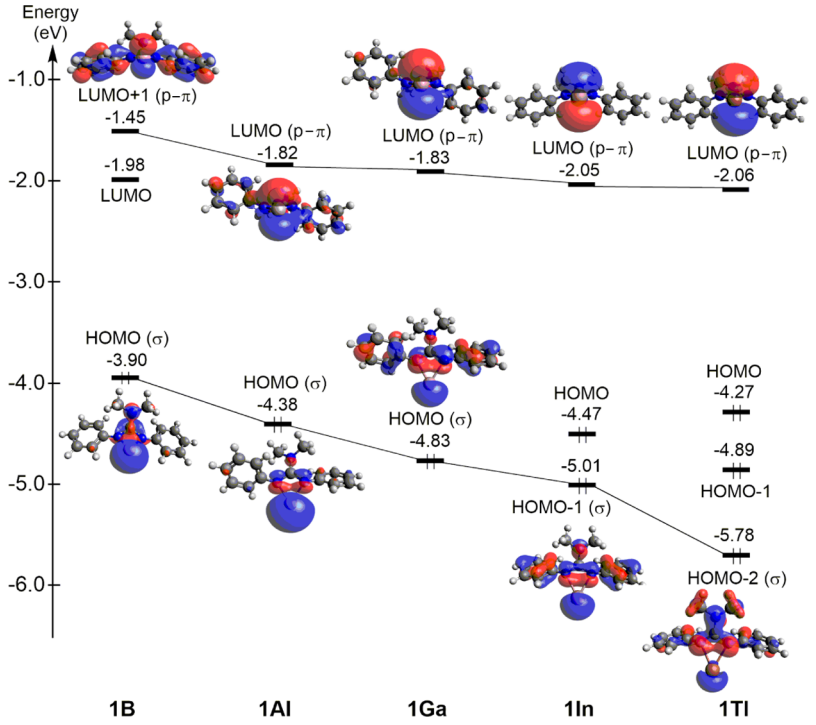

Figure 1. Calculated frontier molecular orbitals of the four-membered **1E** (E = B, Al, Ga, In, and Tl) species. For more information, see the text.

optimized geometries to do the single-point calculations, whose calculated data are collected in Tables S1 and S2. The extent of aromaticity was evaluated via nucleus-independent chemical shift (NICS, NMR = GIAO) calculations at the BP86/def2-SVP level of theory.[42−44] The anisotropy of the induced current density (ACID)[45,46] calculations were performed at the BP86/def2-SVP level as implemented in the Gaussian 16 C.01 package.[47] The Cartesian coordinates of all BP86/def2-SVP stationary points are collected in the Supporting Information.

3. RESULTS AND DISCUSSION

3.1. Geometries and Electronic Structures of 1E (E = B, Al, Ga, In, and Tl). We first ascertained the reliability of the BP86[29,30]/def2-SVP[31−33] method to compute the geometrical structures of the model reactants, **1E**. Selected computed geometric parameters are compared with the available experimental data[20] in Table 1.

As mentioned in the Introduction, to date, only the four-membered NHC counterparts bearing a gallium or indium central atom (Scheme 1) have been successfully synthesized and identified via X-ray spectroscopy.[20] Table 1 shows that the BP86/def2-SVP and experimental[19] Ga−N and In−N bond lengths (Å) differ by approximately 0.072 and 0.080, respectively. Similarly, the theoretical ∠NGaN (63.81°) and ∠NInN (57.68°) bond angles agree well with the corresponding experimental findings (63.77 and 58.06°, respectively).[20] Although the substituents of the **1E** model reactants used in this work are somewhat different from those of the experimental reports, these encouraging results still convince us that the BP86/def2-SVP calculations furnish an adequate foundation for further investigations into the origin of the activation energies for the reactions of four-membered **1E** compounds.

We notice that the central carbenic angle ($\angle N_1-E-N_2$) shown in Table 1 decreases uniformly as E is changed from boron to thallium. This result could be due to a relativistic effect or the so-called "orbital nonhybridization effect" and "inert s-pair effect".[48−51] As the atomic weight of the periodic family element goes from light (such as B) to heavy (such as Tl), its valence s orbital is more strongly contracted than its corresponding p orbitals. This result, in turn, makes the size difference between the valence s and p orbitals increase from B to Tl. As a result, the heavier the central E element in **1E** is, the poorer the overlap between its valence s and p orbitals is, and the smaller its central carbenic angle is. Our computational data listed in Table 1 confirm this prediction, that is, $\angle N_1-B-N_2$ (87.88°) > $\angle N_1-Al-N_2$ (65.62°) > $\angle N_1-Ga-N_2$ (63.81°) > $\angle N_1-In-N_2$ (57.78°) > $\angle N_1-Tl-N_2$ (54.63°).

Our BP86/def2-SVP results provided in Table 1 show that the singlet−triplet energy splitting values ΔE_{st} (= $E_{triplet} - E_{singlet}$) for **1B**, **1Al**, **1Ga**, **1In**, and **1Tl** are 10.9, 43.9, 50.6, 53.1, and 54.5 kcal/mol, respectively, that is, ΔE_{st} increases in the order **0B** < **0Al** < **0Ga** < **0In** < **0Tl**. In other words, our theoretical findings reveal that the heavier the E atom in the neutral four-membered-ring NHC analogue (**1E**) is, the larger the singlet−triplet energy separation (ΔE_{st}) in **1E** will be. The trend in the ΔE_{st} of the **1E** molecules can be readily understood from their valence molecular orbitals based on the BP86/def2-SVP calculations. Figure 1 shows that the HOMO of **1E** is essentially a nonbonding sp^2-σ orbital, except for **1In** (HOMO-1) and **1Tl** (HOMO-2). The electronic manifolds of the last two heavier species may be altered by the "inert s-pair effect" and "orbital nonhybridization effect",[48−51] as stated earlier. Nevertheless, the substitution of one E element in **1E** can result in its LUMO being a p−π orbital, whose orbital energy remains comparatively constant from B to Tl, as shown in Figure 1. As a result, these two effects lead to an increased energy gap between the nonbonding $sp^2-\sigma$ orbital and the vacant p−π orbital for the heavier **1E** species. This increased energy gap, in turn, results in a larger ΔE_{st} energy splitting for the heavier four-membered **1E** compounds.

https://doi.org/10.1021/acsomega.1c02958
ACS Omega 2021, 6, 22272−22283

Our B3LYP computational results show that the four-membered ring of **1E** is planar (Figures S5−S9), which agrees well with the available experimental report.[20] It is noteworthy that the number of the valence electrons in this four-membered NHC analogue (**1E**; Scheme 1) is eight, that is, three lone pairs from nitrogen, one from carbon, and one from a central E element. See Scheme 2. Because the $sp^2-\sigma$ orbital

Scheme 2. Four-Membered Ring of 1E Has Six p−π lectrons in Resonance

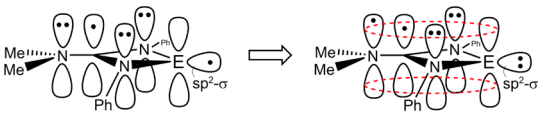

on an E atom contains the s and p orbitals, it means that the orbital energy of this $sp^2-\sigma$ orbital is lower than that of the pure $p-\pi$ orbital on the E element. As a result, two valence electrons must be filled in the $sp^2-\sigma$ orbital. This, in turn, leaves six valence electrons, which can act as six $p-\pi$ electrons on a four-membered ring of **1E**.

The most noteworthy issue of **1E** chemistry is whether its four-membered ring has aromatic character. In fact, it is well accepted that the NICS[42−44] is an effective aromaticity criterion for judging ring molecules. Interestingly, our theoretical examination reveals that these four-membered **1E** molecules can be characterized by their degrees of aromaticity. We computed NICS(0), NICS(1), and NICS(1)zz, as shown in Table 1. All of these data show the same trend, that is, the heavier the central E element in **1E** is, the lower the NICS value (aromaticity) of **1E** will be. For instance, our computational results predict that the NICS(1)zz value of **1E** increases in the order −7.592 (**1B**) < −4.155 (**1Al**) < −1.842 (**1Ga**) < 0.629 (**1In**) < 1.097 (**1Tl**), a trend that is consistent with the atomic number of the central E atom. Therefore, the NICS value of **1B** is the highest among the **1E** species, which means that **1B** has more aromatic character, whereas the four heavier molecules (**1Al**, **1Ga**, **1In**, and **1Tl**) are nonaromatic.[42−44] These results can be ascribed to the atomic radius of the E atom in the four-membered ring of **1E**. Namely, in the four-membered ring of **1B**, the B, C, and N ring atoms are second-row elements. Hence, the valence 2p orbitals of these atoms are quite similar in size and therefore overlap each other. This result, in turn, leads to aromaticity for **1B**, featuring the highest NICS(1)zz value. On the other hand, the valence np ($n \geq 3$) orbitals of a heavier E′ (= Al, Ga, In, and Tl) are larger than the valence 2p orbitals of the second-row elements. As a result, the overlaps between the former and the latter orbitals are quite poor. This circumstance, in turn, results in nonaromaticity for the four heavier **1E′** molecules, which possess NCIS values that are slightly less negative or slightly positive, as shown in Table 1.

To obtain more evidence of the aromatic or nonaromatic behavior of **1E**, the ACID method[45,46] was used. The ACID method can provide a visualization of the density of delocalized electrons and quantify conjugation effects.[45,46] Figure 2 presents the ACID isosurface of the **1E** molecules at an isosurface contour value of 0.05. We observe that **1B** has a strong aromatic character because the current density vectors in **1B** form a closed circle in the four-membered ring and no disconnection. However, in the other four **1E** (E = Al, Ga, In, and Tl) molecules, each topology of delocalized electrons exhibits two clear disconnections, demonstrating the nonaromatic character of the four-membered rings of the heavier **1E** species.

$$(1\mathbf{E})H^+_{(g)} \rightarrow 1\mathbf{E}_{(g)} + H^+ \quad (3)$$

To understand the basicity of **1E**, one can easily calculate its PA and GB,[52] defined as the enthalpy change for eq 3, which represents a quantitative measure of the intrinsic basicity of **1E** in the gas phase. In principle, the intrinsic basicity of **1E** is due to the availability of its sp^2 lone pair, which can be found in Figure 1. Table 1 indicates that the PA and GB decrease in the order **1B** > **1Al** > **1Ga** > **1In** > **1Tl**, following the inverse of the trend in the atomic radius of the central atom E.[53] The higher

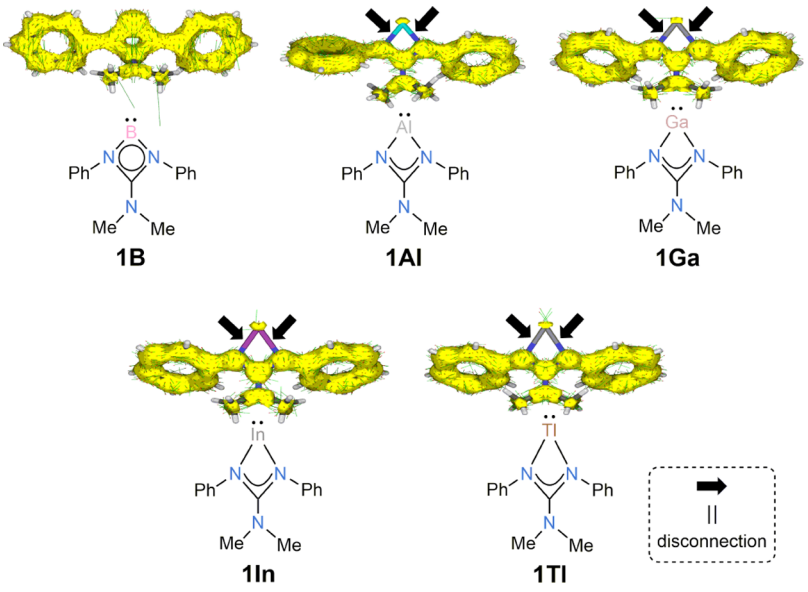

Figure 2. ACID plots for the four-membered **1E** (E = B, Al, Ga, In, and Tl) species. The current density vectors (green arrows with red tips) are plotted onto an isosurface of contour value 0.05. See the text.

https://doi.org/10.1021/acsomega.1c02958
ACS Omega 2021, 6, 22272−22283

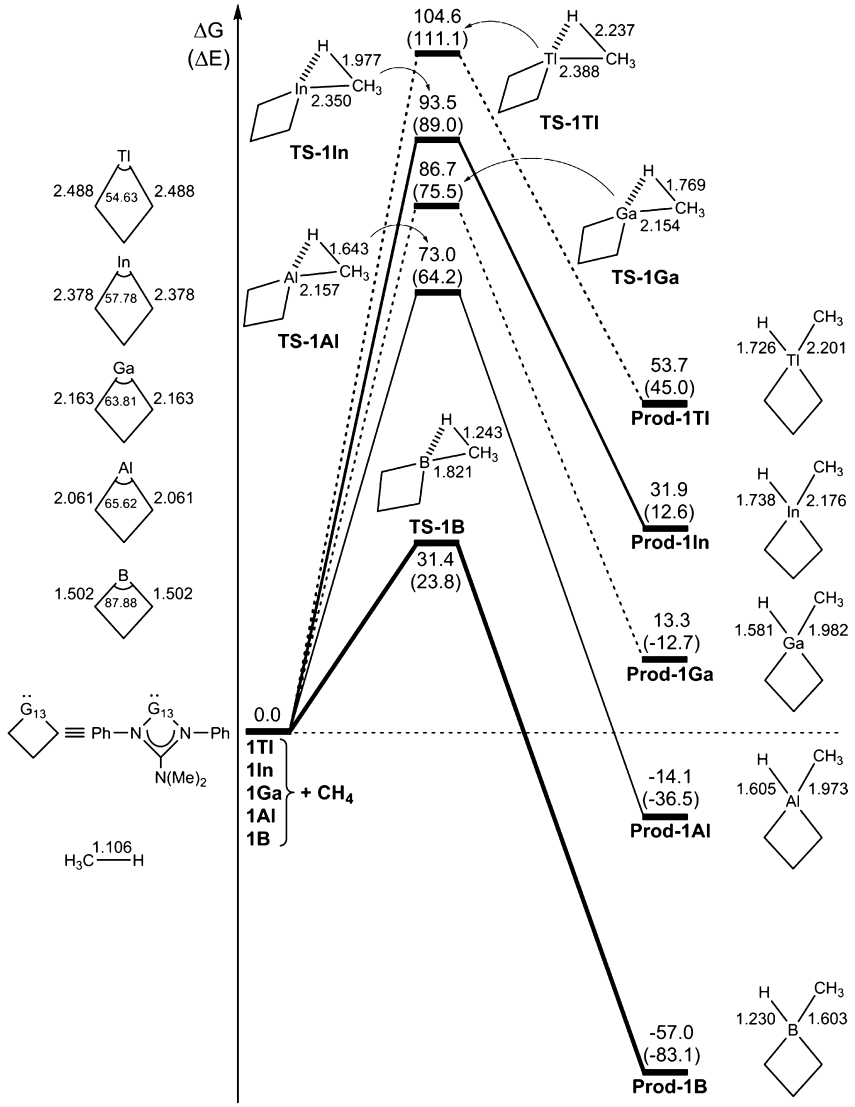

Figure 3. Energy profiles (energy in kcal/mol and bond distances in Å) for the insertion reaction of **1E** (E = B, Al, Ga, In, and Tl) with CH_4. The calculated relative free energies (BP86/def2-SVP) and electronic energies (M06-2X-D3(BJ)/def2-TZVP//BP86/def2-SVP; in parentheses) at the level are given in kcal/mol.

the basicity of **1E** is, the more reactive **1E** will be. As a consequence, our BP86 results from Table 1 strongly suggest that the chemical reactivity of **1E** decreases uniformly as its E is changed from boron to thallium.

We are also interested in the electrophilicity[54] of the **1E** molecule. Based on Koopmans' theorem,[55] the electronic chemical potential (μ) and chemical hardness (η) can be defined as in eqs 4 and 5, respectively.

$$\mu = -\frac{E_{HOMO} + E_{LUMO}}{2} \quad (4)$$

$$\eta = E_{LUMO} - E_{HOMO} \quad (5)$$

As a result, the electrophilicity index (ω), defined by Parr and co-workers,[56] is written as

$$\omega = \frac{\mu^2}{2\eta} \quad (6)$$

Our BP86 data given in Table 1 indicate that the electrophilicity (ω) of **1E** increases in the order **1B** (0.736) < **1Al** (0.777) < **1Tl** (0.793) < **1In** (0.816) < **1Ga** (0.833). If a low electrophilicity is obtained for the most reactive carbene species, then the chemical reactivity is controlled by the lone pair donation ability of this carbene. In contrast, if a high electrophilicity is obtained, then the reactivity is governed by the vacant p−π orbital of this carbene. The above computational data indicate that the sp^2 lone pair orbital found in their HOMO presented in Figure 1 plays a central role in the chemical reactions of **1B** and **1Al**. However, the vacant p−π orbital of **1Ga**, **1In**, and **1Tl**, which is located in the LUMO, as shown in Figure 1, determines the chemical reactivity of these species. These theoretical conclusions are consistent with the observations for aromaticity and basicity discussed above.

Additionally, the Fukui function,[57] the central site reactivity index of DFT, on the carbenic atom (E) of **1E** can be calculated using the following equations (q represents the atomic charge).

$$\text{For nucleophilic attack: } f_k^+ = q_k(N+1) - q_k(N) \quad (7)$$

$$\text{For electrophilic attack: } f_k^- = q_k(N) - q_k(N-1) \quad (8)$$

https://doi.org/10.1021/acsomega.1c02958
ACS Omega 2021, 6, 22272−22283

For radical attack: $f_k^0 = \frac{1}{2}[f_k^+ + f_k^-]$ (9)

Table 1 shows that the Fukui function of nucleophilic attack (f_k^+) has a higher value than that of electrophilic attack (f_k^-) for both **1B** and **1Al**, which strongly suggest that their sp^2 lone pair governs their chemical reactions. In contrast, the other three molecules (**1Ga**, **1In**, and **1Tl**) have higher values of electrophilic attack (f_k^-) than those of nucleophilic attack (f_k^+). As a result, the vacant p−π orbital of the three heavier **1E** species plays an important role in their chemical reactions. In other words, the Fukui function is an appropriate indicator of the nature of the reactivity of **1E**. Again, the above theoretical findings are consistent with the above theoretical results for the aromaticity, basicity, and electrophilicity.

We shall use the concepts of the above electronic factors to search for their relationships with the chemical reactivity of such four-membered-ring NHC analogues (**1E**) in the next section.

3.2. Insertion Reaction of 1E (E = B, Al, Ga, In, and Tl) with Methane. The first chemical reaction of **1E** investigated in this work is eq 1, the insertion reaction of **1E** with methane. The BP86/def2-SVP potential energy surfaces of five **1E** molecules are schematically shown in Figure 3. The calculated activation free energy (ΔG_{ACT}; kcal/mol) of the transition state increases in the order 31.4 (**TS1B**) < 73.0 (**TS1Al**) < 86.7 (**TS1Ga**) < 93.5 (**TS1In**) < 104.6 (**TS1Tl**). Additionally, the free energy (ΔG; kcal/mol) of the final insertion product increases in the order −57.0 (**Prod-1B**) < −14.1 (**Prod-1Al**) < 13.3 (**Prod-1Ga**) < 31.9 (**Prod-1In**) < 53.7 (**Prod-1Tl**). Accordingly, our theoretical findings suggest that **1E** cannot undergo the CH_4 insertion reaction from kinetic and thermodynamic viewpoints. In addition, the above theoretical evidence reveals that the relative chemical reactivity of **1E** decreases in the order **1B** ≫ **1Al** > **1Ga** > **1In** > **1Tl**.

According to the study by Boehme and Frenking,[28] the aromaticity of the NHC ring plays a significant role in stabilizing the cyclic NHC system. Moreover, the antiaromatic species exhibits a higher reactivity than the aromatic one.[58] To determine the origin of the barrier height of the **1E** insertion reaction with methane, we combined the concepts of aromaticity and the activation energy. Apparently, if the vacant p−π orbital of the E element of **1E** is involved in the activation transition state, then its ring resonance can be destroyed, which eliminates the aromaticity and makes the NICS value of **TS1-E** less negative or slightly positive. This result, in turn, causes a larger activation barrier and makes the **1E** moiety less reactive. Figure 4 shows the effect of electron delocalization of the four-membered ring of **1E** along the reaction coordinate of methane activation. As seen in Figure 4, the NICS(1)zz value of **1E** increases from the reactant to its corresponding transition state (**TS-1E**), suggesting that the aromaticity of **1E** is ruined during its activation reaction with methane. The NICS(1)zz value of **TS-1E** increases in the order: **TS-1B** (−4.496) < **TS-1Al** (−2.213) < **TS-1Al** (−1.182) < **TS-1In** (3.892) < **TS-1Tl** (4.185), whose trend is the same as that of its CH_4 activation barriers, as shown in Figure 3. These facts strongly imply that when **1E** undergoes the insertion reaction with CH_4, strong interactions occur between orbitals. In other words, our theoretical investigation shows that the frontier vacant p−π orbital of **1E** interacts greatly with the orbitals of CH_4 in **TS-1E** bearing a heavier E element. This result, in turn,

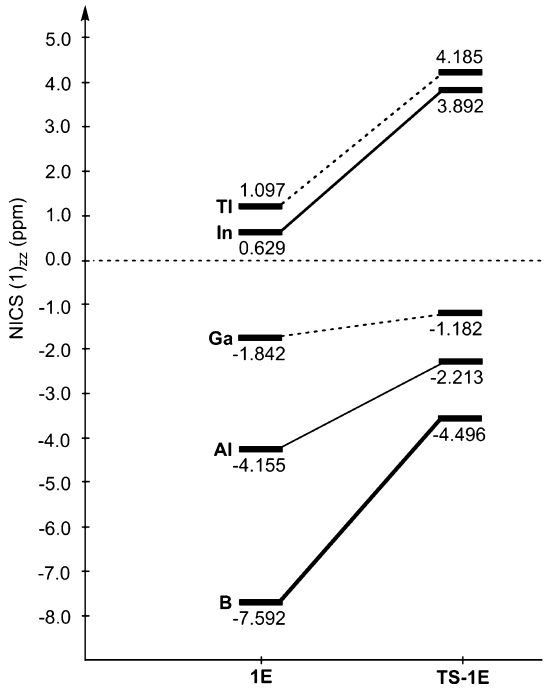

Figure 4. NICS(1)zz values of the four-membered ring from the reactants (**1E**) to the corresponding transition states (**TS1-E**).

can increase the NICS value of its four-membered ring and then retard its methane insertion reaction.

Figure 5 demonstrates that each ACID[45,46] topology of delocalized electrons in **TS1E** has two disconnections between the E and N atoms of the four-membered ring. This theoretical evidence strongly indicates that regardless of the aromaticity of the **1E** molecule, its four-membered ring character would be greatly destroyed by the insertion reaction with methane, which is already reflected in the NICS values presented in Figure 4. This result, in turn, would lead to a larger reaction barrier height, making its C−H bond activation reaction unfeasible. Accordingly, our theoretical observations strongly suggest that the aromatic criterion of **1E** can act as a measure in determining the reactivity of the four-membered group 13 NHC counterparts (**1E**) with methane.

Moreover, our theoretical findings concerning the frontier molecular orbitals, basicity, electrophilicity, and Fukui function discussed earlier reveal that for the lighter **1B** molecule, its sp^2 lone pair orbital (HOMO in Figure 1) plays a predominant role in determining its chemical reactivity. On the contrary, the vacant p−π orbital (LUMO in Figure 1) of the heavier **1E′** (E′ = Al, Ga, In, and Tl) species has a major influence on their chemical reactivity. In other words, the nature of the chemical bonding of **1B** reflects a higher basicity and nucleophilicity than those of the four heavier **1E** molecules.

To further understand the key factors that influence the barrier heights of the insertion reactions of **1E** with methane, an activation strain model (ASM)[59−62] was used in this study. Table 2 shows that the activation energy (ΔE_{ACT}) can be divided into two deformation energies ($\Delta E_{DEF,CH4} + \Delta E_{DEF,1E}$) and one binding energy (ΔE_{BIND}). In eq 1, a H_3C−H bond cleavage accompanies the formation of the H_3C-**1E** and the H-**1E** bonds. The calculated H_3C···H distances and the H_3C···**1E** distances in the transition state (**TS1E**) are shown in Figure 3. Figure 6 schematically shows the trends in the theoretical data (ΔE_{ACT}, $\Delta E_{DEF,CH4}$, $\Delta E_{DEF,1E}$, and ΔE_{BIND}) taken from Table

https://doi.org/10.1021/acsomega.1c02958
ACS Omega 2021, 6, 22272−22283

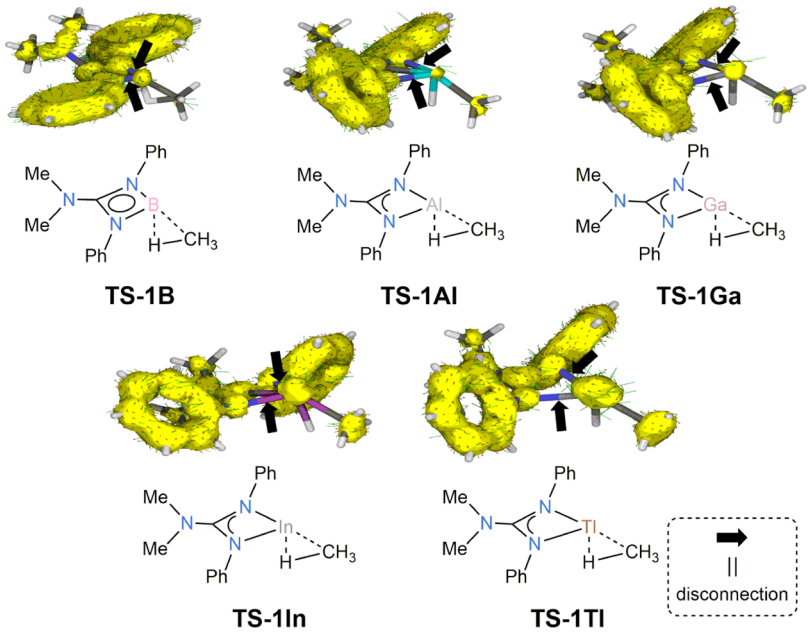

Figure 5. ACID plots for the **TS-1E** (E = B, Al, Ga, In, and Tl) point. The current density vectors (green arrows with red tips) are plotted onto the isosurface of contour value 0.05. See the text.

Table 2. Energy Decomposition Analysis of Methane Activation by 1E (E = Group 13 Elements) Calculated at the M06-2X-D3(BJ)/def2-TZVP//BP86/def2-SVP Level of Theory

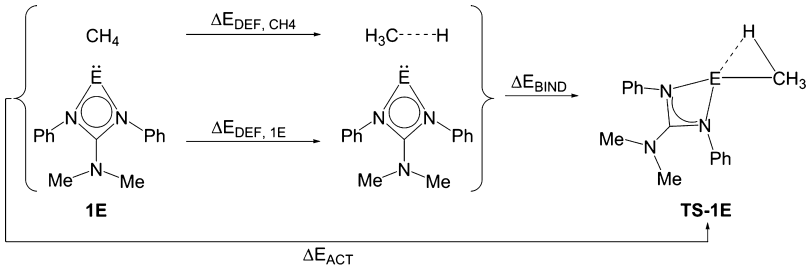

entry	TS-1B	TS-1Al	TS-1Ga	TS-1In	TS-1Tl
ΔE_{ACT}[a,b]	23.8	64.2	75.5	89.0	111.1
$\Delta E_{DEF,CH_4}$	17.0	63.0	78.4	92.7	112.5
$\Delta E_{DEF,1E}$	16.9	6.3	−1.1	0.9	5.3
ΔE_{BIND}	−10.1	−5.1	−1.8	−4.6	−6.7

[a] $\Delta E_{ACT} = \Delta E_{DEF,CH_4} + \Delta E_{DEF,1E} + \Delta E_{BIND}$. [b] All in kcal mol^{-1}.

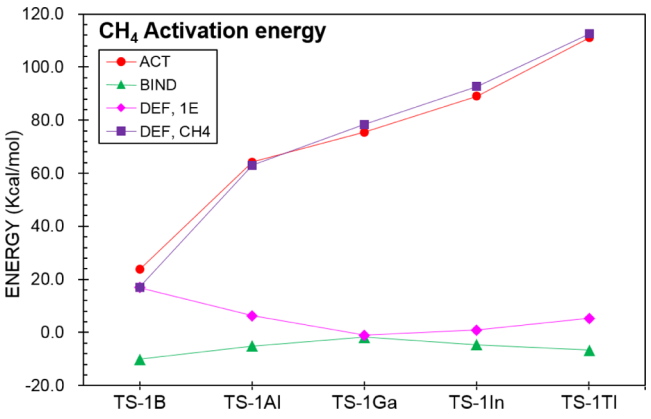

Figure 6. Energy decompositions of the activation energies (ΔE_{ACT}) of the transition states (**TS-1E**) of the insertion reactions of **1E** (E = group 13 element) with CH_4. The data are taken from Table 2.

2. Figure 6 reveals that $\Delta E_{DEF,CH4}$ is a decisive factor affecting the activation energy (ΔE_{ACT}). The deformation energy $\Delta E_{DEF,CH4}$ presented in Figure 6 increases monotonically from **TS-1B** to **TS-1Tl**, a trend that is consistent with the corresponding activation energies. The reason why $\Delta E_{DEF,CH4}$ increases monotonically from boron to thallium can be understood from the geometrical structures of **TS-1E**. Figure 3 shows that the transition state H_3C-H bond distance (Å) increases in the order 1.243 (**TS-1B**) < 1.643 (**TS-1Al**) < 1.769 (**TS-1Ga**) < 1.977 (**TS-1In**) < 2.237 (**TS-1Tl**), while the original H_3C-H bond distance of methane is 1.106 Å. Notably, the atomic radius of E increases in the order B (84 pm) < Al (121 pm) < Ga (122 pm) < In (142 pm) < Tl (148 pm).[53]

We have also probed the origin of the thermodynamic results for these insertion reactions shown in Figure 3. The sum of the bond orders (WBI)[62] of two newly formed bonds (i.e., E−H and E−CH_3) in the **1E** compound were calculated

https://doi.org/10.1021/acsomega.1c02958
ACS Omega 2021, 6, 22272−22283

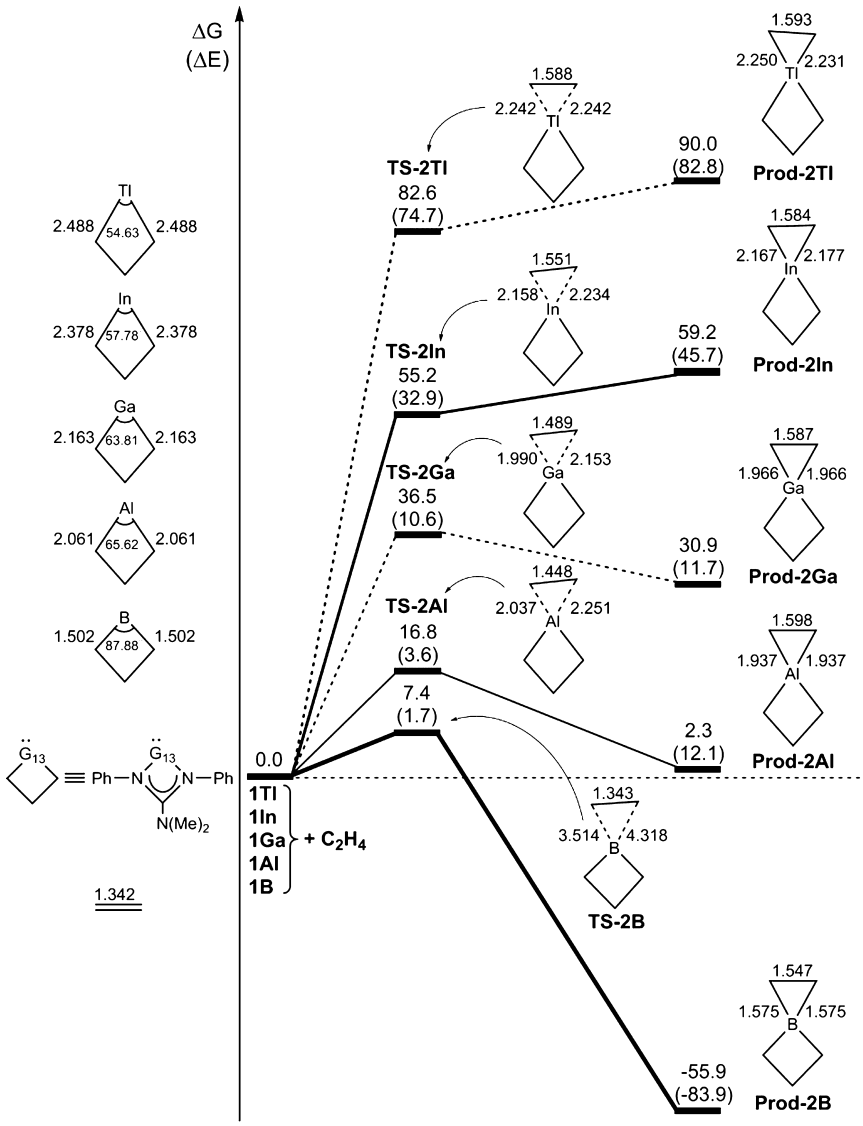

Figure 7. Energy profiles (energy in kcal/mol and bond distances in Å) for the [1 + 2] cycloaddition reaction of **1E** (E = B, Al, Ga, In, and Tl) with C_2H_4. The calculated relative free energies (BP86/def2-SVP) and electronic energies [M06-2X-D3(BJ)/def2-TZVP//BP86/def2-SVP; in parentheses] at the level are given in kcal/mol.

to decrease in the order 1.871 (**1B**) > 1.651 (**1Al**) > 1.554 (**1Ga**) > 1.520 (**1In**) > 1.469 (**1Tl**). This trend is consistent with that of the reaction enthalpies of **1E** presented in Figure 3. Accordingly, our BP86 calculated results suggest that the insertion products for the heavier **1E** molecules are thermodynamically less stable than those for the lighter **1E** ones. These theoretical results are again explicable in terms of the atomic radius of the central E in the four-membered group 13 NHC analogue.

3.3. Cycloaddition Reaction of 1E (E = B, Al, Ga, In, and Tl) with Ethene. Next, we investigated the [1 + 2] cycloaddition reaction of **1E** with ethene as represented by eq 2. Similarly, the transition states (**TS2E**) and cycloaddition products (**2E**) were calculated at the BP86/def2-SVP level of theory, whose potential energy surfaces are summarized in Figure 7 accompanied by selected geometrical parameters.

Figure 7 shows that the substitution of an E element in the four-membered NHC increases the [1 + 2] cycloaddition barrier (ΔG_{ACT}; kcal/mol) on going from boron to thallium, that is, **TS2B** (7.4) < **TS2Al** (16.8) < **TS2Ga** (36.5) < **TS2In** (55.2) < **TS2Tl** (82.6). Analogously, this substitution also increases the reaction free energy (ΔG; kcal/mol) down group 13, that is, **2B** (−55.9) < **2Al** (2.3) < **2Ga** (30.9) < **2In** (59.2) < **2Tl** (90.0). The BP86/def2-SVP results indicate that the heavier the E element in the **1E** species is, the higher the activation energy will be, the larger the reaction free energy will be, and the greater the endothermicity of the [1 + 2] cycloaddition reaction with ethene will be. That is, four cycloaddition reaction paths (from **1Al** to **1Tl**) are energetically unfavorable from kinetic and thermodynamic viewpoints. Nevertheless, our computational evidence presented in Figure 7 predicts that only path **1B** + C_2H_4 → **TS-2B** → **Prod-2B** is thermodynamically and kinetically favorable. Again, similar to the methane activation reaction discussed earlier, our theoretical information for the study of the ethene cycloaddition reaction indicates that **1B** and **1Tl** have the highest and lowest reactivities, respectively.

We also analyzed the relationship between the calculated NICS values of **1E** and the activation barriers of its [1 + 2] cycloaddition reaction with ethene. The theoretical data of the

https://doi.org/10.1021/acsomega.1c02958
ACS Omega 2021, 6, 22272−22283

NICSs provide an understanding of the reactivity of such cycloaddition reactions. Our theoretical examination indicates that the trend in the NICS(1)zz values for **1E** is identical to the trends in the activation free energy (ΔG_{ACT}) and reaction free energy (ΔG), as discussed above (Figure 7).

Figure 8 shows the variations in the NICS values of the four-membered ring from the reactants (**1E**) to the corresponding transition states (**TS-2E**). Similar to the previous case of methane activation (Figures 3 and 4), the NICS(1)zz values of **TS-2E** increase in the following order: **TS-2B**(-7.238) < **TS-2Al**(-0.091) < **TS-2Al**(-0.012) < **TS-2In**(3.286) < **TS-2Tl**(3.892), whose trend is the same as that of its ethene activation barriers, as given in Figure 7. Accordingly, our theoretical examination demonstrates that the NICS(1)zz values of the four-membered group 13 NHC analogues can be viewed as a guide to anticipating the order of reactivity of the corresponding [1 + 2] cycloaddition reactions.

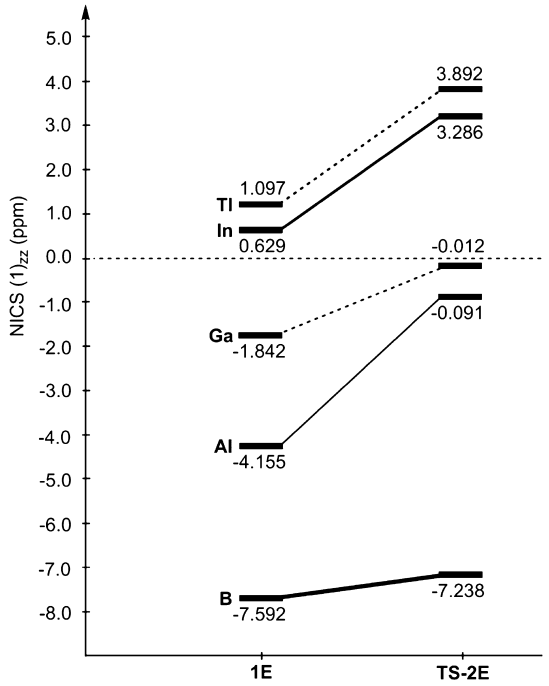

Figure 8. NICS(1)zz values of the four-membered ring from the reactants (**1E**) to the corresponding transition states (**TS-2E**).

Figure 9 presents the ACID[45,46] isosurface of the transition-state structures (**TS2E**) of the [1 + 2] cycloaddition reactions of **1E** and C_2H_4. It is obvious that the current density vectors plotted onto the ACID isosurface of **TS-2B** show the diatropic ring current, which forms a loop around the four-membered ring of the **1B** moiety, as expected for an aromatic system. However, two big disconnections occur in the four-membered rings of the heavier **TS-2E′** (E′ = Al, Ga, In, and Tl) species, which greatly destroy their aromatic character. Moreover, according to the Hammond postulate,[64] because the pattern of the **1B** moiety in **TS-2B** is quite similar to that of the original reactant, the activation barrier for the [1 + 2] cycloaddition reaction with ethene should be much lower than those of the heavier **1E′** molecules. This prediction is already confirmed, as represented in Figure 7.

To further probe the cycloaddition reaction mechanism, the abovementioned ASM[59−62] calculations were used in this work. The ASM computational results are collected in Table 3 and schematically represented in Figure 10. Figure 10 demonstrates that only the curve of the deformation energy of C_2H_4 ($\Delta E_{DEF,C2H4}$) coincides with that of the [1 + 2] cycloaddition barrier height (ΔE_{ACT}). Accordingly, our computational examination reveals that $\Delta E_{DEF,C2H4}$ is a key factor for determining the trend in the activation barriers. Indeed, the BP86/def2-SVP results predict that the C−C bond distance (Å) in **TS-2E** increases in the order 1.343 (**TS-2B**) < 1.448 (**TS-2Al**) < 1.469 (**TS-2Ga**) < 1.551 (**TS-2In**) < 1.588 (**TS-2Tl**), whereas the original BP86/def2-SVP C−C bond length of ethene is 1.342 Å (Figure 7). The monotonic

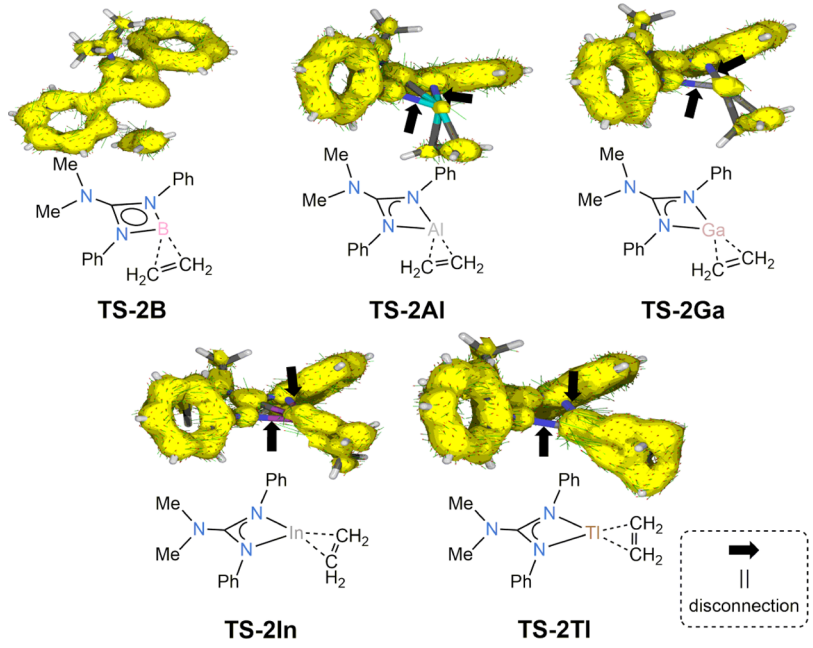

Figure 9. ACID plots for the **TS-2E** (E = B, Al, Ga, In, and Tl) stationary point. The current density vectors (green arrows with red tips) are plotted onto the isosurface of contour value 0.05. See the text.

https://doi.org/10.1021/acsomega.1c02958
ACS Omega 2021, 6, 22272−22283

Table 3. Energy Decomposition Analysis of Ethene Activation by 1E (E = Group 13 Elements) Calculated at the M06-2X-D3(BJ)/def2-TZVP//BP86/def2-SVP Level of Theory

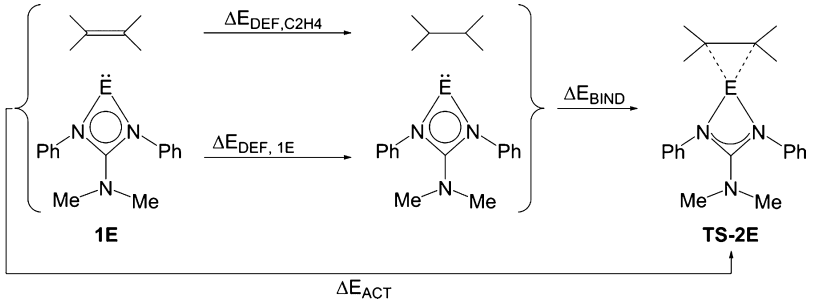

entry	TS-2B	TS-2Al	TS-2Ga	TS-2In	TS-2Tl
ΔE_{ACT} [a,b]	1.7	3.6	10.6	32.9	74.7
$\Delta E_{DEF,C_2H_4}$	2.5	11.7	22.2	37.5	71.4
$\Delta E_{DEF,1E}$	2.4	3.1	1.5	10.1	20.5
ΔE_{BIND}	−3.2	−11.2	−13.1	−14.7	−17.2

[a] $\Delta E_{ACT} = \Delta E_{DEF,CH4} + \Delta E_{DEF,1E} + \Delta E_{BIND}$. [b] All in kcal mol^{-1}.

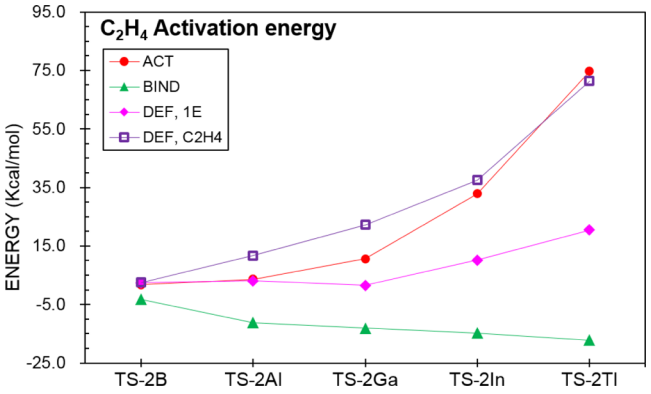

Figure 10. Energy decompositions of the activation energies (ΔE_{ACT}) of the transition states (**TS-2E**) of the [1 + 2] cycloaddition reactions of **1E** (E = group 13 element) with C_2H_4. The data are taken from Table 3.

increase in the curves from **TS-2B** to **TS-2Tl** can be attributed to the atomic size of the E element in **1E**. As stated earlier, the atomic radius increases down group 13.[57] To gain a better orbital overlap between E and the two carbon atoms in ethene, the C−C bond length in ethene must be increased. This greater deformation results in the higher activation barriers, as discussed above.

Again, as discussed above, our theoretical observations reveal that during the [1 + 2] cycloaddition reaction of **1E** with C_2H_4, the lighter **1B** species has the lowest activation barrier and the greatest exothermicity of the final cycloproduct (**Prod-2B**). In addition to the atomic radius of the central boron atom, the high reactivity of **1B** can also be attributed to its stronger basicity and nucleophilicity than those of the other four **1E′** (E′ = Al, Ga, In, and Tl) molecules.

In addition, we investigated the origin of the thermodynamic outcome for the final cycloaddition products, **Prod-2E**. After examining the sum of the bond orders (WBI)[63] of two newly formed key bonds (i.e., E−CH_2), our DFT calculations demonstrate that the sums of these bond orders decrease in the order 1.737 (**Prod-2B**) > 1.508 (**Prod-2Al**) > 1.496 (**Prod-2Ga**) > 1.434 (**Prod-2In**) > 1.331 (**Prod-2Tl**). That is, to obtain a better overlap between the central group 13 atom (E) and the carbon atoms of the attacking ethene, the larger the atomic radius of E in **1E** is, the longer the C−C bond of the reacting ethene is in the final product, and the higher the endothermicity of the cycloaddition reaction will be.

4. CONCLUSIONS

In summary, with the help from the concepts of electronic factors in the four-membered ring group 13 NHC analogues and the ASM[59−62] method, herein, we report an approach to obtaining a better understanding of the origin of the activation barriers of the C−H bond insertion reaction with methane and the [1 + 2] cycloaddition reaction with ethene. The present theoretical findings predict that the chemical reactivity of the four-membered-ring **1E** carbenes decreases in the order **1B** ≫ **1Al** > **1Ga** > **1In** > **1Tl**. In addition, our theoretical analysis demonstrates that the NICS values can be a diagnostic criterion for anticipating the relative reactivity of four-membered ring 13 NHC analogues.

The present theoretical examination also demonstrates that among the four-membered **1E** molecules, the lighter **1B** features the highest basicity and a high nucleophilicity, whereas the four heavier **1E′** species possess a lower basicity but larger electrophilicity. This is because the former species uses its nonbonding sp^2 lone pair orbital as the HOMO to govern its chemical reactivity, while the latter four species use the vacant p−π orbital as the LUMO to determine their chemical reactivity. Besides, this work reveals that using the NICS values, which measure the aromatic character of the four-membered ring of **1E**, can be a tool to predict the relative order of its chemical reactivity.

It is hoped that this work can help experimental chemists open new synthetic methods and new applications for the four-membered ring group 13 NHC analogues.

■ ASSOCIATED CONTENT

Supporting Information

The Supporting Information is available free of charge at https://pubs.acs.org/doi/10.1021/acsomega.1c02958.

Optimized geometries and the absolute energies (in Hartrees) for all the points on the potential energy surfaces of 1E, TS-1E, Prod-1E, TS-2E, and Prod-2E (E = B, Al, Ga, In, and Tl) at the BP86/Def2-SVP, M06-2X/def2-SVP//BP86/def2-SVP, B3LYP/LANL2DZ

https://doi.org/10.1021/acsomega.1c02958
ACS Omega 2021, 6, 22272−22283

+dp//BP86/def2-SVP, and BP86-D3(BJ)/Def2-TZVP//BP86/Def2-SVP levels of theory (PDF)

AUTHOR INFORMATION

Corresponding Author

Ming-Der Su − *Department of Applied Chemistry, National Chiayi University, Chiayi 60004, Taiwan; Department of Medicinal and Applied Chemistry, Kaohsiung Medical University, Kaohsiung 80708, Taiwan;* orcid.org/0000-0002-5847-4271; Email: midesu@mail.ncyu.edu.tw

Author

Zheng-Feng Zhang − *Department of Applied Chemistry, National Chiayi University, Chiayi 60004, Taiwan*

Complete contact information is available at: https://pubs.acs.org/10.1021/acsomega.1c02958

Author Contributions

Z.-F.Z. conducted all of the theoretical computations and analyzed the results. M.-D.S. supervised the research activities and contributed to the manuscript preparation. Two authors regularly discussed the progress of the research, reviewed the manuscript, and gave approval for the final version.

Notes

The authors declare no competing financial interest.

ACKNOWLEDGMENTS

The authors are grateful to the National Center for High-Performance Computing of Taiwan in providing huge computing resources to facilitate this research. They also thank the Ministry of Science and Technology of Taiwan for the financial support. Special thanks are also due to reviewers 1, 2, 3, and 4 for very helpful suggestions and comments.

REFERENCES

(1) Kirmse, W. *Carbene Chemistry*, 1st ed.; Academic Press: New York, 1964, Chapter 1.

(2) Arduengo, A. J., III; Harlow, R. L.; Kline, M. A stable crystalline carbene. *J. Am. Chem. Soc.* **1991**, *113*, 361−363.

(3) For annual reviews: Crabtree, R. H. Recent developments in the organometallic chemistry of N-heterocyclic carbenes. *Coord. Chem. Rev.* **2007**, *251*, 595−895.

(4) For annual reviews: Arduengo, A. J.; Bertrand, G. Carbenes Introduction. *Chem. Rev.* **2009**, *109*, 3209−3884.

(5) For annual reviews: Vashi, P. The Way Forward with N-Heterocyclic Carbenes. *Eur. J. Inorg. Chem.* **2009**, 1663−2007.

(6) For annual reviews: Ekkehardt Hahn, F. Introduction to themed issue on N-heterocyclic carbenes. *Dalton Trans.* **2009**, *38*, 6873.

(7) Martin, D.; Melaimi, M.; Soleilhavoup, M.; Bertrand, G. A Brief Survey of Our Contribution to Stable Carbene Chemistry. *Organometallics* **2011**, *30*, 5304−5313.

(8) See for example: Flanigan, D. M.; Romanov-Michailidis, F.; White, N. A.; Rovis, T. Organocatalytic Reactions Enabled by N-Heterocyclic Carbenes. *Chem. Rev.* **2015**, *115*, 9307−9387.

(9) See for example: Zhong, R.; Lindhorst, A. C.; Groche, F. J.; Kühn, F. E. Immobilization of N-Heterocyclic Carbene Compounds: A Synthetic Perspective. *Chem. Rev.* **2017**, *117*, 1970−2058.

(10) See for example: Huynh, H. V. Electronic Properties of N-Heterocyclic Carbenes and Their Experimental Determination. *Chem. Rev.* **2018**, *118*, 9457−9492.

(11) See for example: Nesterov, V.; Reiter, D.; Bag, P.; Frisch, P.; Holzner, R.; Porzelt, A.; Inoue, S. NHCs in Main Group Chemistry. *Chem. Rev.* **2018**, *118*, 9678−9842.

(12) See for example: Peris, E. Smart N-Heterocyclic Carbene Ligands in Catalysis. *Chem. Rev.* **2018**, *118*, 9988−10031.

(13) See for example: Doddi, A.; Peters, M.; Tamm, M. N-Heterocyclic Carbene Adducts of Main Group Elements and Their Use as Ligands in Transition Metal Chemistry. *Chem. Rev.* **2019**, *119*, 6994−7112.

(14) See for example: Vivancos, Á.; Segarra, C.; Albrecht, M. Mesoionic and Related Less Heteroatom-Stabilized N-Heterocyclic Carbene Complexes: Synthesis, Catalysis, and Other Applications. *Chem. Rev.* **2018**, *118*, 9493−9586.

(15) See for example: Kuwata, S.; Hahn, F. E. Complexes Bearing Protic N-Heterocyclic Carbene Ligands. *Chem. Rev.* **2018**, *118*, 9642−9677.

(16) See for example: Danopoulos, A. A.; Simler, T.; Braunstein, P. N-Heterocyclic Carbene Complexes of Copper, Nickel, and Cobalt. *Chem. Rev.* **2019**, *119*, 3730−3961.

(17) See for example: Smith, C. A.; Narouz, M. R.; Lummis, P. A.; Singh, I.; Nazemi, A.; Li, C.-H.; Crudden, C. M. N-Heterocyclic Carbenes in Materials Chemistry. *Chem. Rev.* **2019**, *119*, 4986−5056.

(18) See for example: Zhao, Q.; Meng, G.; Nolan, S. P.; Szostak, M. N-Heterocyclic Carbene Complexes in C−H Activation Reactions. *Chem. Rev.* **2020**, *120*, 1981−2048.

(19) See for example: Jazzar, R.; Soleilhavoup, M.; Bertrand, G. Cyclic (Alkyl)- and (Aryl)-(amino)carbene Coinage Metal Complexes and Their Applications. *Chem. Rev.* **2020**, *120*, 4141−4168.

(20) Jones, C.; Junk, P. C.; Platts, J. A.; Stasch, A. Four-Membered Group 13 Metal(I) N-Heterocyclic Carbene Analogues: Synthesis, Characterization, and Theoretical Studies. *J. Am. Chem. Soc.* **2006**, *128*, 2206−2207.

(21) Findlater, M.; Hill, N. J.; Cowley, A. H. Synthesis and structure of two new (guanidinate)boron dichlorides and their attempted conversion to boron(I) derivatives. *Dalton Trans.* **2008**, *37*, 4419−4423.

(22) Jones, C.; Junk, P. C.; Platts, J. A.; Rathmann, D.; Stasch, A. Synthesis, characterisation and theoretical studies of amidinato-indium(I) and thallium(I) complexes: isomers of neutral group 13 metal(I) carbene analogues. *Dalton Trans.* **2005**, *34*, 2497−2499.

(23) Green, S. P.; Jones, C.; Stasch, A. Homo- and heteroleptic complexes of four-membered group 13 metal(I) n-heterocyclic carbine analogues with group 10 metal(0) fragments. *Inorg. Chem.* **2007**, *46*, 11−13.

(24) Jin, G.; Jones, C.; Junk, P. C.; Stasch, A.; Woodul, W. D. Group 13 metal(I) and (II) guanidinate complexes: effect of ligand backbone on metal oxidation state and coordination sphere. *New J. Chem.* **2008**, *32*, 835−842.

(25) Jones, C.; Stasch, A.; Moxey, G. J.; Junk, P. C.; Deacon, G. B. Complexes of four-membered group 13 metal(I) n-heterocyclic carbene analogues with metal carbonyl fragments. *Eur. J. Inorg. Chem.* **2009**, *2009*, 3593−3599.

(26) Moxey, G. J.; Jones, C.; Stasch, A.; Junk, P. C.; Deacon, G. B.; Woodul, W. D.; Drago, P. R. Complexes of four-membered group 13 metal(I) n-heterocyclic carbene analogues with platinum(II) fragments. *Dalton Trans.* **2009**, *38*, 2630−2636.

(27) Overgaard, J.; Jones, C.; Dange, D.; Platts, J. A. Experimental charge density analysis of a gallium(I) n-heterocyclic carbene analogue. *Inorg. Chem.* **2011**, *50*, 8418−8426.

(28) Boehme, C.; Frenking, G. Electronic Structure of Stable Carbenes, Silylenes, and Germylenes. *J. Am. Chem. Soc.* **1996**, *118*, 2039−2046.

(29) Becke, A. D. Density-functional exchange-energy approximation with correct asymptotic behavior. *Phys. Rev. A: At., Mol., Opt. Phys.* **1988**, *38*, 3098−3100.

(30) Perdew, J. P. Density-functional approximation for the correlation energy of the inhomogeneous electron gas. *Phys. Rev. B: Condens. Matter Mater. Phys.* **1986**, *33*, 8822−8824.

(31) Weigend, F.; Ahlrichs, R. Balanced basis sets of split valence, triple zeta valence and quadruple zeta valence quality for H to Rn: Design and assessment of accuracy. *Phys. Chem. Chem. Phys.* **2005**, *7*, 3297−3305.

(32) Schäfer, A.; Horn, H.; Ahlrichs, R. Fully optimized contracted Gaussian basis sets for atoms Li to Kr. *J. Chem. Phys.* **1992**, *97*, 2571−2577.
(33) Metz, B.; Stoll, H.; Dolg, M. Small-core multiconfiguration-Dirac-Hartree-Fockadjusted pseudopotentials for post-d main group elements: Application to PbH and PbO. *J. Chem. Phys.* **2000**, *113*, 2563−2569.
(34) Fukui, K. Formulation of the reaction coordinate. *J. Phys. Chem.* **1970**, *74*, 4161−4163.
(35) Fukui, K. The path of chemical reactions—the IRC approach. *Acc. Chem. Res.* **1981**, *14*, 363−368.
(36) Gonzalez, C.; Schlegel, H. B. An improved algorithm for reaction path following. *J. Chem. Phys.* **1989**, *90*, 2154−2161.
(37) Grimme, S.; Ehrlich, S.; Goerigk, L. Effect of the damping function in dispersion corrected density functional theory. *J. Comput. Chem.* **2011**, *32*, 1456−1465.
(38) Grimme, S.; Antony, J.; Ehrlich, S.; Krieg, H. A Consistent and Accurate Ab Initio Parametrization of Density Functional Dispersion Correction (DFT-D) for the 94 Elements H-Pu. *J. Chem. Phys.* **2010**, *132*, 154104−154122.
(39) Weigend, F.; Ahlrichs, R. Balanced basis sets of split valence, triple zeta valence and quadruple zeta valence quality for H to Rn: Design and assessment of accuracy. *Phys. Chem. Chem. Phys.* **2005**, *7*, 3297−3305.
(40) Zhao, Y.; Truhlar, D. G. Density Functionals with Broad Applicability in Chemistry. *Acc. Chem. Res.* **2008**, *41*, 157−167.
(41) Weigend, F. Accurate Coulomb-fitting basis sets for H to Rn. *Phys. Chem. Chem. Phys.* **2006**, *8*, 1057−1065.
(42) Schleyer, P. v. R.; Maerker, C.; Dransfeld, A.; Jiao, H.; van Eikema Hommes, N. J. R. Nucleus-Independent Chemical Shifts: A Simple and Efficient Aromaticity Probe. *J. Am. Chem. Soc.* **1996**, *118*, 6317−6318.
(43) Chen, Z.; Wannere, C. S.; Corminboeuf, C.; Puchta, R.; Schleyer, P. v. R. Nucleus-Independent Chemical Shifts (NICS) as an Aromaticity Criterion. *Chem. Rev.* **2005**, *105*, 3842−3888.
(44) Psciuk, B. T.; Lord, R. L.; Winter, C. H.; Schlegel, H. B. Can Metallapyrimidines Be Aromatic? A Computational Study into a New Class of Metallacycles? *J. Chem. Theory Comput.* **2012**, *8*, 4950−4959.
(45) Herges, R.; Geuenich, D. Delocalization of electrons in molecules. *J. Phys. Chem. A* **2001**, *105*, 3214−3220.
(46) Geuenich, D.; Hess, K.; Köhler, F.; Herges, R. Anisotropy of the induced current density (ACID), a general method to quantify and visualize electronic delocalization. *Chem. Rev.* **2005**, *105*, 3758−3772.
(47) Frisch, M. J.; Trucks, G. W.; Schlegel, H. B.; Scuseria, G. E.; Robb, M. A.; Cheeseman, J. R.; Scalmani, G.; Barone, V.; Mennucci, B.; Petersson, G. A.; Nakatsuji, H.; Caricato, M.; Li, X.; Hratchian, H. P.; Izmaylov, A. F.; Bloino, J.; Zheng, G.; Sonnenberg, J. L.; Hada, M.; Ehara, M.; Toyota, K.; Fukuda, R.; Hasegawa, J.; Ishida, M.; Nakajima, T.; Honda, Y.; Kitao, O.; Nakai, H.; Vreven, T.; Montgomery, J. A., Jr.; Peralta, J. E.; Ogliaro, F.; Bearpark, M.; Heyd, J. J.; Brothers, E.; Kudin, K. N.; Staroverov, V. N.; Keith, T.; Kobayashi, R.; Normand, J.; Raghavachari, K.; Rendell, A.; Burant, J. C.; Iyengar, S. S.; Tomasi, J.; Cossi, M.; Rega, N.; Millam, J. M.; Klene, M.; Knox, J. E.; Cross, J. B.; Bakken, V.; Adamo, C.; Jaramillo, J.; Gomperts, R.; Stratmann, R. E.; Yazyev, O.; Austin, A. J.; Cammi, R.; Pomelli, C.; Ochterski, J. W.; Martin, R. L.; Morokuma, K.; Zakrzewski, V. G.; Voth, G. A.; Salvador, P.; Dannenberg, J. J.; Dapprich, S.; Daniels, A. D.; Ortiz, J. V.; Cioslowski, R. L.; Martin, K.; Morokuma, O.; Farkas, O.; Foresman, J. B.; Fox, D. J. *Gaussian 16*, Revision C.01; Gaussian, Inc.: Wallingford, CT, 2016.
(48) Pyykko, P.; Desclaux, J. P. Relativity and the periodic system of elements. *Acc. Chem. Res.* **1979**, *12*, 276−281.
(49) Kutzelnigg, W. Chemical Bonding in Higher Main Group Elements. *Angew. Chem., Int. Ed.* **1984**, *23*, 272−295.
(50) Pyykkö, P. Relativistic effects in structural chemistry. *Chem. Rev.* **1988**, *88*, 563−594.
(51) Pyykkö, P. Strong Closed-Shell Interactions in Inorganic Chemistry. *Chem. Rev.* **1997**, *97*, 597−636.
(52) Betowski, L. D.; Solomon, J. J.; Porter, R. F. Proton affinity of borazine. *Inorg. Chem.* **1972**, *11*, 424−427.
(53) Cordero, B.; Gómez, V.; Platero-Prats, A. E.; Revés, M.; Echeverría, J.; Cremades, E.; Barragán, F.; Alvarez, S. Covalent radii revisited. *Dalton Trans.* **2008**, *37*, 2832−2838.
(54) Chattaraj, P. K.; Sarkar, U.; Roy, D. R. Electrophilicity Index. *Chem. Rev.* **2006**, *106*, 2065−2091.
(55) Koopmans, T. A. Über die Zuordnung von Wellenfunktionen und Eigenwerten zu den Einzelnen Elektronen Eines Atoms. *Physica* **1934**, *1*, 104−113.
(56) Parr, R. G.; Szentpály, L. v.; Liu, S. Electrophilicity Index. *J. Am. Chem. Soc.* **1999**, *121*, 1922−1924.
(57) Ayers, P. W.; Parr, R. G. Variational Principles for Describing Chemical Reactions: The Fukui Function and Chemical Hardness Revisited. *J. Am. Chem. Soc.* **2000**, *122*, 2010−2018.
(58) Levandowski, B. J.; Abularrage, N. S.; Raines, R. T. Differential Effects of Nitrogen-Substitution in 5- and 6-membered Aromatic Motifs. *Chem.—Eur. J.* **2020**, *26*, 8829.
(59) Ziegler, T.; Rauk, A. On the calculation of bonding energies by the Hartree Fock Slater method. *Theor. Chim. Acta* **1977**, *46*, 1−10.
(60) van Zeist, W.-J.; Bickelhaupt, F. M. The activation strain model of chemical reactivity. *Org. Biomol. Chem.* **2010**, *8*, 3118−3127.
(61) Bickelhaupt, F. M.; Houk, K. N. Analyzing Reaction Rates with the Distortion/Interaction-Activation Strain Model. *Angew. Chem., Int. Ed.* **2017**, *56*, 10070−10086.
(62) Fernández, I.; Bickelhaupt, F. M. The activation strain model and molecular orbital theory: understanding and designing chemical reactions. *Chem. Soc. Rev.* **2014**, *43*, 4953−4967.
(63) Glendening, E. D.; Badenhoop, J. K.; Reed, A. E.; Carpenter, J. E.; Bohmann, J. A.; Morales, C. M.; Weinhold, F. *NBO 5.0*; Theoretical Chemistry Institute, University of Wisconsin: Madison, WI, 2001, http://www.chem.wisc.edu/nbo5.
(64) Hammond, G. S. Correlation of Reaction Rates. *J. Am. Chem. Soc.* **1955**, *77*, 334−338.

https://doi.org/10.1021/acsomega.1c02958
ACS Omega 2021, 6, 22272−22283